



Article

Physical–Chemical Exfoliation of *n*-Alkylamine Derivatives of Layered Perovskite-like Oxide $\text{H}_2\text{K}_{0.5}\text{Bi}_{2.5}\text{Ti}_4\text{O}_{13}$ into Nanosheets

Iana A. Minich ¹, Oleg I. Silyukov ^{1,*}, Sergei A. Kurnosenko ¹, Veronika V. Gak ¹, Vladimir D. Kalganov ², Petr D. Kolonitskiy ³ and Irina A. Zvereva ¹

¹ Department of Chemical Thermodynamics and Kinetics, Institute of Chemistry, Saint Petersburg State University, 199034 Saint Petersburg, Russia; st048953@student.spbu.ru (I.A.M.); st040572@student.spbu.ru (S.A.K.); st062004@student.spbu.ru (V.V.G.); irina.zvereva@spbu.ru (I.A.Z.)

² Interdisciplinary Resource Centre for Nanotechnology, Saint Petersburg State University, 199034 Saint Petersburg, Russia; v.kalganov@spbu.ru

³ Centre for Innovative Technologies of Composite Nanomaterials, Saint Petersburg State University, 199034 Saint Petersburg, Russia; petr.kolonitckii@spbu.ru

* Correspondence: oleg.silyukov@spbu.ru



Citation: Minich, I.A.; Silyukov, O.I.; Kurnosenko, S.A.; Gak, V.V.; Kalganov, V.D.; Kolonitskiy, P.D.; Zvereva, I.A. Physical–Chemical Exfoliation of *n*-Alkylamine Derivatives of Layered Perovskite-like Oxide $\text{H}_2\text{K}_{0.5}\text{Bi}_{2.5}\text{Ti}_4\text{O}_{13}$ into Nanosheets. *Nanomaterials* **2021**, *11*, 2708. <https://doi.org/10.3390/nano11102708>

Academic Editors: Juan Francisco Sánchez Royo and Arthur P. Baddorf

Received: 15 August 2021

Accepted: 5 October 2021

Published: 14 October 2021

Publisher's Note: MDPI stays neutral with regard to jurisdictional claims in published maps and institutional affiliations.



Copyright: © 2021 by the authors. Licensee MDPI, Basel, Switzerland. This article is an open access article distributed under the terms and conditions of the Creative Commons Attribution (CC BY) license (<https://creativecommons.org/licenses/by/4.0/>).

Abstract: In the present work, we report the results on exfoliation and coating formation of inorganic–organic hybrids based on the layered perovskite-like bismuth titanate $\text{H}_2\text{K}_{0.5}\text{Bi}_{2.5}\text{Ti}_4\text{O}_{13} \cdot \text{H}_2\text{O}$ that could be prepared by a simple ion exchange reaction from a Ruddlesden–Popper phase $\text{K}_{2.5}\text{Bi}_{2.5}\text{Ti}_4\text{O}_{13}$. The inorganic–organic hybrids were synthesized by intercalation reactions. Exfoliation into nanosheets was performed for the starting hydrated protonated titanate and for the derivatives intercalated by *n*-alkylamines to study the influence of preliminary intercalation on exfoliation efficiency. The selected precursors were exfoliated in aqueous solutions of tetrabutylammonium hydroxide using facile stirring and ultrasonication. The suspensions of nanosheets obtained were characterized using UV–vis spectrophotometry, dynamic light scattering, inductively coupled plasma spectroscopy, and gravimetry. Nanosheets were coated on preliminarily polyethyleneimine-covered Si substrates using a self-assembly procedure and studied using atomic force and scanning electron microscopy.

Keywords: layered oxides; perovskites; bismuth titanates; exfoliation; nanosheets; coating

1. Introduction

Two-dimensional materials obtained from bulk materials have become an important research topic since the inception of graphene technologies [1]. One of the most promising directions in this field is the production of nanolayers via topdown approaches such as the exfoliation of bulk layered oxides. In particular, layered compounds with a perovskite structure are of great interest.

Layered perovskite-like oxides consist of negatively charged perovskite-like layers that fold into a two-dimensional layered structure with cations occupying the interlayer space to compensate for the negative charge of the layers [2,3]. In recent years, layered perovskite-like oxides have attracted great attention due to their structural features and associated anisotropic physical effects. Such compounds exhibit various interesting functional properties such as superconductivity [4,5], dielectric, ferroelectric and piezoelectric properties [6–10], photoluminescence [11–13], and photocatalytic activity [14–17]. In addition, as a rule, they demonstrate high thermal and mechanical stability and can be relatively easily and economically obtained via high-temperature solid-phase synthesis methods [18]. It is important to note that these materials allow useful characteristics to be fine-tuned, since the A sites of layered perovskites can be easily modified with metal ions using a conventional solid-state method [11,19–23].

Such compounds can replace interlayer cations of alkali metals by ion exchange with other cations, in particular, cations of other metals, complex cationic units, or protons,

which, in the latter case, allows one to obtain so-called protonated forms [24–27]. One of the significant features of the protonated forms of perovskite-like oxides is their acidic properties, which allow the intercalation of organic bases to be conducted into their interlayer space, forming organic–inorganic hybrids [27–30]. Some perovskite-like oxides have been successfully exfoliated into two-dimensional perovskite nanosheets using chemical exfoliation in solutions of bulky quaternary ammonium ions [13,31–34]. Oxide nanosheets (about 1 nm thick) with the perovskite structure have completely different physical properties than their bulk counterparts. They can serve as multipurpose precursors for creating multilayer films, porous composites, and layered nanocomposites [33,35–38]. The resulting nanolayers already show intriguing properties with potential uses in photoluminescence [39,40], catalysis [16,41–43], and energy storage [44,45].

Even though for some layered perovskite-like oxides, the processes of protonation and subsequent splitting into nanolayers have been studied in great detail, the number of known structures amenable to exfoliation remains rather limited. In this regard, the task of finding new similar compounds is important.

Recently Liu et al. [46] synthesized a new layered Ruddlesden–Popper phase $K_{2.5}Bi_{2.5}Ti_4O_{13}$ (KBT_4) with mixed K/Bi co-occupancy on the perovskite A site, showing stoichiometric hydration and being amenable to form protonated compounds $H_2K_{0.5}Bi_{2.5}Ti_4O_{13} \cdot yH_2O$ [47,48] via substitution of K^+ by H^+ . The $H_2K_{0.5}Bi_{2.5}Ti_4O_{13} \cdot H_2O$ ($HKBT_4 \cdot H_2O$) structure can be described as an alternation of perovskite slabs ($K_{0.5}Bi_{2.5}Ti_4O_{13}$) with interlayer protons and water molecules. It was shown that this protonated derivative is capable of intercalation of *n*-alkylamines [49] and grafting of *n*-alcohols in the interlayer space [50]. This work reports on exfoliating $HKBT_4 \cdot H_2O$ and its *n*-alkylamine derivatives in a tetrabutylammonium hydroxide (TBAOH) aqueous solution to obtain stable suspensions of perovskite nanolayers and their coatings.

2. Materials and Methods

2.1. Sample Preparation and Characterization

2.1.1. Initial Substances

KNO_3 (Vekton, St Petersburg, Russia, 99.9%), Bi_2O_3 (Vekton, St Petersburg, Russia, 99.9%), and TiO_2 (Vekton, St Petersburg, Russia, 99.9%) were dried at 200, 600, and 1000 °C, respectively. Methylamine ($MeNH_2$, 38% solution in water, Chemical line, St Petersburg, Russia), ethylamine ($EtNH_2$, 70% solution in water, Merck, Darmstadt, Germany), *n*-propylamine ($PrNH_2$, Sigma-Aldrich, St Louis, MI, USA, 98%), *n*-butylamine ($BuNH_2$, 99.9%, Chemical line, St Petersburg, Russia), *n*-hexylamine ($HxNH_2$, Sigma-Aldrich, St Louis, MI, USA, 99.9%), *n*-heptane (ECOS, Moscow, Russia, 99.9%), TBAOH (40 wt. % solution in water, Acros Organics, NJ, USA); polyethyleneimine (PEI, approx. M.N. 60,000, branched, 50 wt. % solution in water, Acros Organics, NJ, USA) were used as received.

Preparation of Inorganic Hosts

The starting inorganic matrix, KBT_4 , and its protonated form were prepared by previously reported methods [46,48]. KBT_4 was synthesized using a solid-state reaction from Bi_2O_3 , TiO_2 , and KNO_3 . The oxides were taken in stoichiometric ratios; the 20% excess of KNO_3 was used to compensate for its loss during the calcination due to the volatilization. $HKBT_4 \cdot H_2O$ was obtained via the ion exchange reaction, which was carried out for 1 week in 1M HNO_3 at 20 °C.

Preparation of Inorganic–Organic Hybrids

Inorganic–organic hybrids with *n*-amines $HKBT_4 \times RNH_2$ were obtained by acid–base intercalation in solutions of corresponding *n*-amines. The reactions were performed in optimized conditions reported earlier. [49] Namely, hybrids with methylamine, ethylamine, *n*-propylamine, and *n*-butylamine were obtained via the 24 h reaction at 60 °C using 38% (for methylamine) and 50% aqueous solutions. The reaction with *n*-hexylamine was

performed at 80 °C in 50% solution in *n*-heptane. After the reactions, solid products were washed with acetone or *n*-hexane (for HxNH₂ derivative).

2.1.2. Precursors Characterization

The fact of formation and phase purity of the precursors prepared were controlled using XRD analysis. The detailed qualitative and quantitative characterization of hydrated and dehydrated protonated forms obtained and *n*-alkylamine intercalated hybrids were performed via XRD, Raman, FTIR, and ¹³C NMR spectroscopy, and TG, STA, and CNH analysis, details of which we presented earlier [50]. Starting from the ethylamine derivative, the intercalation of *n*-alkylamines led to a linear increase in the interlayer distance, *d*, compared to that of the hydrated protonated sample, which confirms the fact of the intercalation and the resulting weakening of direct binding of perovskite layers to each other.

2.1.3. Exfoliation

The protonated and amine-intercalated forms obtained were exfoliated using a physical–chemical method that implies the ultrasound treatment of the precursors in an aqueous solution of TBAOH. Specifically, the solid samples were taken in amounts according to a TBA⁺:H⁺ ratio of 1:1 and suspended in 30 mL of 0.004M TBAOH. The suspensions were sonicated using an ultrasonic homogenizer (UP200St) equipped with a 7 mm sonotrode (Hielscher, Teltow, Germany) at a half ultrasound amplitude, A = 50%, for 5 min (total energy ~8000 Ws) twice with intermediate stirring of the suspension at room temperature (~20 °C) for 24 h and 1 week. After the second sonication step, the fraction of large particles containing an unexfoliated residue was separated using centrifugation at 1000 RCF for 60 min.

2.1.4. Concentration Determination

The concentration of suspension was studied firstly by two direct approaches—inductively coupled plasma spectrometry (ICP) analysis and the gravimetry method for the suspension obtained from the *n*-butylamine precursor (for higher concentrations, A = 100% sonication was used). It should be noted that the concentration of obtained suspensions for other layered compounds presented in the literature is often disregarded [31,34,51], and, in several works, it is determined by one of these direct methods [13,39,52]. However, the concentration of the suspensions is of high importance for their future applications and specifically for composite preparations and nanosheets' deposition.

Gravimetry was performed as follows: the liquid phase was evaporated at 300 °C in a platinum crucible, preliminarily calcined at 900 °C to constant mass. Then, the sediment was calcined at 800 °C for 10 min several times until constant mass was reached. The temperature was chosen according to the complete decomposition of the protonated form into K_{0.5}Bi_{2.5}Ti₄O₁₃. For ICP analysis, the suspension was mineralized under microwave-assisted heating in a concentrated HNO₃/HF mixture. It was found that, in general, the gravimetric method shows slightly higher concentrations compared to ICP analysis. Higher values calculated for K⁺ content compared to Bi³⁺ and Ti⁴⁺ may be explained by possible incomplete mineralization of the sample. Thus, for further express determination of the concentration, we prepared spectrophotometric calibrations using the nanosheets' concentration determined by the gravimetric method.

To control and compare the efficiency of exfoliation for different precursors, spectrophotometry calibrations based on those obtained by direct methods concentrations were prepared. For this, the suspension was diluted 5, 10, 15, 20, 25, 35, and 50 times using a 0.004 M TBAOH solution. The UV–vis spectra and calibrations prepared are shown in Figure A1. As may be seen, the shape of the bands upon dilutions is preserved, and two clear shoulders with maximums at 215 and 248 nm are presented. Two spectral maximums were compared, and the maximum at 248 nm was used for the calibration equation.

Density calibration was also considered as an alternative method that is less dependent on the particles' size distribution and their morphology. It was found that, in this

case, the dependence is also close to linear in the concentration range studied and, therefore, densimetry may be used as a versatile approach to the suspensions' analysis. The densimetry calibrations obtained are presented in Figure A2.

2.1.5. Sample Preparation for SEM and AFM Measurements

For further characterization of the nanosheets using SEM and AFM methods, their deposition and flocculation were performed. Nanoparticle reassembly for SEM characterization was carried out following the previously reported method via drop-casting of 1M KCl solution [53]. The precipitate obtained was separated by centrifugation, washed with distilled H₂O, and dried under CaO.

Nanosheets' deposition on Si wafers was performed using the self-assembly method shown earlier for other layered niobates and titanates [37,53]. The deposition of the nanosheets was optimized by varying the pH and concentration of the suspensions. The tested concentrations for the original pH (11.9) were 25, 50, 100, 250, 500 and 750 mg/L. Additionally, deposition for suspensions with pH = 9 and concentrations 25, 50, and 100 mg/L was performed. Silicon substrates were washed via treatment in 50% HCl/methanol solution at 60 °C for 30 min and the surface was hydroxylated using concentrated H₂SO₄ for 30 min at 60 °C. After that, for better adhesion of negatively charged nanosheets, the surface of the substrate was coated with positively charged polymer, PEI, via treatment with 2.5 g/L of its aqueous solution at pH = 9. The coating time was 20 min, according to methods outlined in the literature [37,53]. After coating, the wafers were washed with water and calcined at 250 °C for 30 min to remove surface-adsorbed residual TBAOH. Additionally, the reliability of the coating technique was confirmed with the quartz crystal microbalance–dissipation (QCM-D) experiments. The experiments were carried out on SiO₂-coated quartz resonators, with a fundamental vibration frequency of 5 MHz. A detector was fixed in the cell with deionized water. The baseline drift was less than 0.1 Hz/h (which corresponds to 1.77 ng/sm²). The experiment procedure was as follows: firstly, deionized water was replaced by PEI solution, and the cell was left for 20 min to form the coating; then, the stability of the PEI coating obtained was tested in a flow of water, after which the cell was filled with TBAOH solution. The results of QCM-D experiments showed that PEI coating is already formed after two minutes of treatment. The water flow leads to the partial diffusion of the PEI from the surface; after that, the coating is stabilized. Treatment of the sensor with the TBAOH solution leads to a similar effect caused by the adsorption of TBAOH molecules.

2.2. Instrumentation

Powder X-ray diffraction (XRD) analysis of the samples was performed on a Rigaku Miniflex II benchtop diffractometer (Tokyo, Japan) with CuK α radiation, angle range, $2\theta = 3 - 60^\circ$, scanning rate, $10^\circ/\text{min}$, step, 0.02° . The lattice parameters were calculated on the basis of all the reflections observed using DiffracPlus Topas software (Bruker, Billerica, MA, USA). Concentrations of perovskite nanosheets in colloidal solutions used for building spectrophotometric calibration plots were determined by inductively coupled plasma atomic emission spectroscopy (ICP) on a Shimadzu ICPE-9000 spectrometer (Shimadzu, Kyoto, Japan) after preliminary acid digestion. Spectrophotometric analysis was performed on a Thermo Scientific GENESYS 10S UV–Vis spectrophotometer (Waltham, MA, USA). The pH values of nanosheets suspensions' media were measured using a laboratory pH-meter Toledo SevenCompact S220 (Mettler Toledo, Greifensee, Switzerland) equipped with an InLab Expert Pro-ISM electrode. Particle size distribution in colloidal suspensions, as well as their ζ -potentials, were determined using the method of dynamic light scattering (DLS) on a Photocor Compact-Z analyzer (Photocor, Moscow, Russia) using DynaLS software (version, Photocor, Moscow, Russia). Morphology of the coated particles was investigated on a Zeiss Merlin (Oberkochen, Germany) scanning electron microscope (SEM). Particle thickness and surface topography were studied using an NT-MDT Integra-Aura (manufacturer, Zelenograd, Russia) atomic-force microscope (AFM) and Gwyddion

software (version,, Czech Metrology Institute, Brno, Czech Republic). Quartz crystal microbalance-dissipation experiments were performed on a BiolinScientific Q-Sense E-4 (BiolinScientific, Gothenburg, Sweden) device.

3. Results and Discussion

3.1. Optimization of Suspensions Preparations

In the present work, physical–chemical exfoliation was used. This approach implies two driving forces for exfoliation: the intercalation of the bulky exfoliation agent into the interlayer space, which facilitates the intercalation of solvent molecules and leads to the swelling of the sample, and subsequent sonication, which generates cavitation bubbles, resulting in high temperature and pressure local zones, which break apart the original samples' blocks into nanosheets. To determine the impact of these factors on the exfoliation efficiency and to optimize the conditions to prepare highly concentrated suspensions, we considered a row of samples with varied interlayer molecules, namely an as-prepared protonated form, which only includes water molecules in the interlayer space and organically modified samples with preliminarily intercalated *n*-amines: methylamine, ethylamine, *n*-propylamine, *n*-butylamine, and *n*-hexylamine. In addition, the duration of the intermediate stirring between sonication steps was varied for some of the samples.

Examples of UV–vis spectra, obtained for the suspensions of protonated and *n*-amine-intercalated samples with 24 h holding, are presented in Figure 1. As it may be seen in the case of organically modified precursors Me-Bu, two wide shoulders with maximums at 215 and 248 nm are presented on spectral bands, which may be the result of the size distribution of particles in the suspension. In the case of the protonated and *n*-hexylamine samples, a sharp peak at 210 nm appears. It should also be noted that visible agglomeration was detected for these suspensions, which was later additionally confirmed by DLS measurements for the dispersed protonated form. So, we associate the appearance of this band with the formation of bigger spherical agglomerates providing different scattering effects. In the case of the *n*-hexylamine sample, the floating and poor mixing of the powder in the TBAOH water solution were observed, which is most possibly caused by the strong hydrophobicity of the surface-adsorbed *n*-hexylamine. Although, as it may be seen from the spectra, sonication still made its partial exfoliation possible, implied by the presence of the wide shoulder, as in the case of other *n*-amine intercalates. The sample obtained was strongly unstable and the residue of floating agglomerates could not be separated by centrifugation, so this sample is not considered further in this work.

The concentrations of the suspensions prepared from the row of amine-intercalated samples with intermediate stirring for 24 h and 1 week are presented in Table 1. In the case of 24 h experiments, exfoliation was performed three times with different precursors, prepared under the same conditions, and the average concentration is presented. As it may be seen, the concentration insignificantly varies for suspensions, prepared using stirring for 24 h and 1 week, so it may be concluded that the insertion of exfoliant and solvents molecules is not time-dependent for these samples. In contrast, the choice of precursor for exfoliation strongly influences the exfoliation efficiency. In all of the cases, the most concentrated suspensions could be prepared using the *n*-propylamine and *n*-butylamine intercalates. The highest nanosheet concentration achieved using the *n*-propylamine derivative was about 780 mg/L. Earlier, we tested other Ruddlesden–Popper titanates, HLnTiO_4 and $\text{H}_2\text{Ln}_2\text{Ti}_3\text{O}_{10}$ ($\text{Ln} = \text{La}, \text{Nd}$) [54], the exfoliation of which was more efficient for the methylamine derivatives in comparison with *n*-butylamine ones, so we expected similar results for the present bismuth titanate. This was mainly explained by the stronger methylamine affinity to water, compared to less hydrophilic longer-chain *n*-amines, which leads to the more effective intercalation of water molecules during the stirring period, promoting subsequent exfoliation. Another possible reason may be associated with stronger alkyl–alkyl interactions between alkyl chains in the interlayer space for larger *n*-amines, preventing the lamination of the layered structure. The present work uses similar approaches to compare the exfoliation process for two different matrices and, as a result, it may be

concluded that the choice of precursor for each matrix should be found experimentally rather than theoretically.

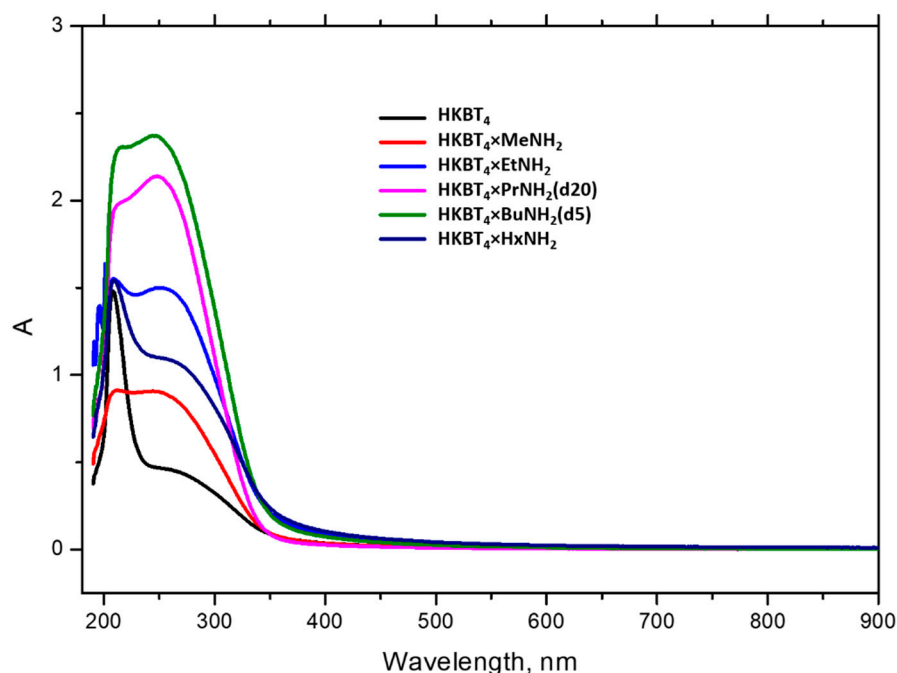


Figure 1. UV-vis spectra of suspensions obtained from protonated titanate $\text{HKBT}_4 \cdot \text{H}_2\text{O}$ and its inorganic-organic hybrids.

Table 1. Concentrations of suspensions obtained from various inorganic-organic hybrids with 24 h and 1 week intermediate stirring time calculated from UV-vis spectra.

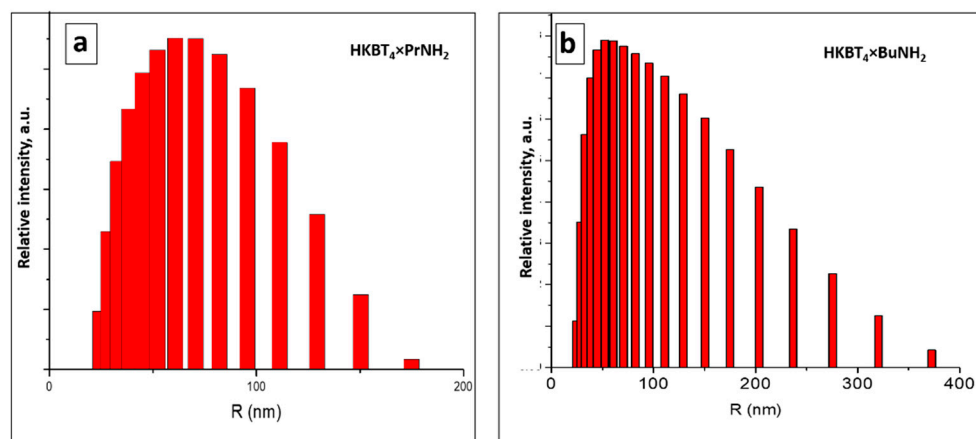
Sample	Concentration (24 h), mg/L	Concentration (1 w), mg/L
$\text{HKBT}_4 \times \text{MeNH}_2$	18	13
$\text{HKBT}_4 \times \text{EtNH}_2$	26	23
$\text{HKBT}_4 \times \text{PrNH}_2$	730	770
$\text{HKBT}_4 \times \text{BuNH}_2$	156	245

3.2. DLS Measurements

Average sizes of particles and size distribution in the suspensions prepared from various precursors, determined by DLS measurements, are shown in Table 2 and Figure 2. DLS measurements were performed for all of the suspensions the next day after preparation, and suspensions were shaken before the measurements. The presented results for samples with the narrowest size distribution (for *n*-propylamine) and wider size distribution (for *n*-butylamine) are refracted in the calculated average size for each sample. As it may be seen, in all of the cases, the average particle sizes were about 100 nm, except for slightly decreased sizes for $\text{HKBT}_4 \times \text{PrNH}_2$ suspension. The poor stability of the suspension prepared from protonated sample led to the aggregation of the particles into $\sim 2 \mu\text{m}$ agglomerates after 24 h. However, the resonication right before the measurement shows that the original sizes of the particles correlate with the ones for amine-containing samples.

Table 2. Average sizes of prepared nanoparticles in suspensions determined by DLS.

Sample	Average Size, nm
HKBT ₄ (aggregated)	~2000
HKBT ₄ (resonicated)	96
HKBT ₄ × MeNH ₂	77
HKBT ₄ × EtNH ₂	83
HKBT ₄ × PrNH ₂	65
HKBT ₄ × BuNH ₂	88

**Figure 2.** Particles size distribution for selected (a) *n*-propylamine and (b) *n*-butylamine non-aggregated samples.

3.3. Stability of Nanoparticles Suspensions

The stability of the suspensions obtained is an important characteristic defining the possibility of their storage and practical use. Moreover, stability should be considered for the further deposition of particles. In addition to visual and spectrometric control of suspension stability over time and during centrifugation (as we use centrifugation to separate unexfoliated residue, it also serves as a factor of the detected “exfoliation efficiency”), the aggregative stability of suspensions was also evaluated by measuring zeta potentials. ζ -potentials were measured for as-prepared suspensions from various precursors and for suspensions, prepared from protonated and *n*-propylamine intercalated forms at different pHs. ζ -potentials for suspensions prepared from various amine-intercalated precursors are presented in Figure 3a. As it may be seen, the ζ values obtained vary in the range from -17 to -27 mV, which corresponds to the average stability of metal oxide suspensions. However, the concentrated suspensions obtained did not show any visible agglomeration after 2 months of undisturbed storage (in the case of Me-Bu samples).

The main factors affecting ζ -potential considered are the pH of the suspensions, surface conductivity [55], and the concentration of suspensions [56]. It was shown earlier that strong dilution may lead to the lower stability of suspensions, which was observed in the case of the exfoliated protonated form. It should also be noted that the most concentrated suspension obtained using the *n*-propylamine sample showed a similar value for zeta potential. Nevertheless, practically, this suspension showed high stability.

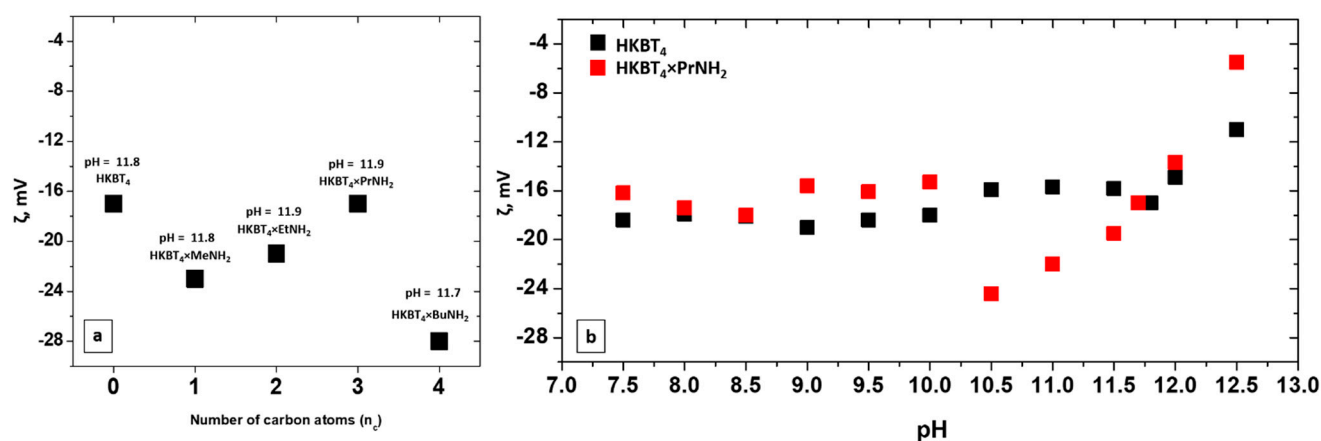


Figure 3. Potentials for (a) suspensions, prepared with various inorganic–organic precursors, (b) HKBT₄ (black) and HKBT₄ × PrNH₂ (red) suspensions with varied pH.

The dependence of ζ -potentials on pH for the suspensions obtained from protonated and *n*-propylamine forms is presented in Figure 3b. In both cases, the original pH of the suspensions was ~11.8–11.9 and it was lowered by the dropwise addition of HCl and raised using a KOH solution. The step was 0.5 and the maximum studied pH was 12.5 due to the visible strong agglomeration of the particles at this pH. Both of the suspensions show similar values of ζ -potentials at their original pH (~17 mV). The values for the protonated sample at pH = 7.5–11.8 vary in the range of ~16–19 mV and the lowering is observed at higher pH with the minimum by module at pH = 12.5 ($\zeta = -11$ mV). A similar plot is obtained for the *n*-propylamine sample in the pH range of 7.5–10 with the local maximum (by module) at pH = 10.5 ($\zeta = -24$ mV). A more crucial decrease in ζ -potential is observed at a high pH with minimal value $\zeta = -5.5$ mV).

The pH of the obtained suspensions was also considered to verify that the difference in stability and obtained concentration does not arise from the difference in pH. In all of the cases, the pH of the suspensions prepared with 24 h stirring was in the range of ~11.7–11.9, which corresponds to the original pH of the TBAOH solution (11.8), while the pH for suspensions prepared with 1 w stirring was found to be in the range of ~9.5–9.9, which implies that pH does not depend on the precursor chosen for exfoliation and the concentration of suspensions obtained. Thus, there is no evident correlation between the pH of suspensions and exfoliation efficiency in the pH range studied.

3.4. Particles Deposition on Silicon Wafers

Deposition of the samples was performed from suspensions prepared using the *n*-propylamine precursor, as they had the highest original concentration. In the self-assembly approach used before for niobates and titanates [37,53], relatively diluted suspensions were used and the pH was usually adjusted to pH = 9, as it favors the presence of a higher percentage of cationic groups in the PEI coating [57]. In this work, we varied the concentration, and in some cases, the pH of suspensions to optimize particles' deposition, as such experiments have not been performed before with bismuth titanates. The efficiency of deposition and the lateral size and thickness of the obtained particles were studied using SEM and AFM. SEM images for selected samples are shown in Figure 4.

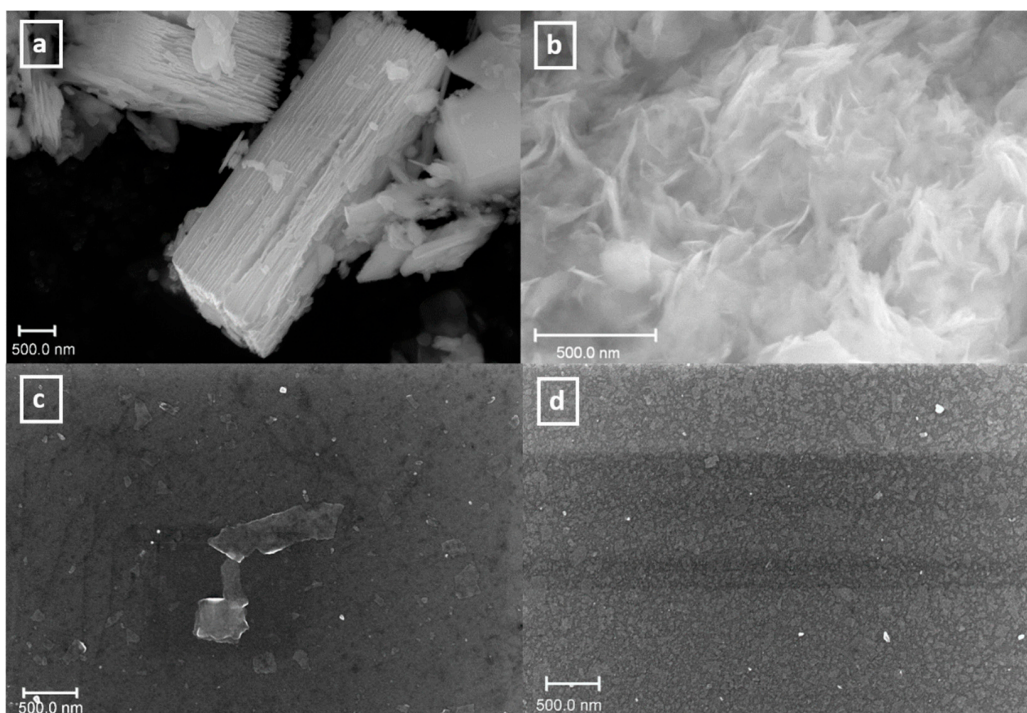


Figure 4. SEM images for initial HKBT₄ PrNH₂ sample (a); reassembled after exfoliation sample (b); Si substrate coating with 50 mg/L suspension at pH = 11.9 (c) and Si substrate coating with 750 mg/L suspension at pH = 11.9 (d).

The bulk powder precursors obtained had a plate-like morphology with relatively big lateral sizes. After exfoliation and reassembly, the agglomerated nanosheets were formed. SEM of the wafers obtained showed that in the case of low concentrations, only some single particles could be detected on the surface and using high concentrations leads to the formation of a more dense coating.

The successful deposition of particles was further proven using AFM. The corresponding images for selected samples are shown in Figure 5.

The deposition of low concentrated samples (25 mg/L) was ineffective and almost no particles were detected on the wafers in both of the cases (at original pH = 11.9 and pH = 9). An increase in suspensions' concentrations generally was shown to result in more dense coatings. Single deposited particles may be observed for the samples, prepared using 50, 100, and 250 mg/L suspensions. The thickness of the particles obtained was found to be in the range of 2.5–5 nm, which corresponds to the monolayers and bilayers of the starting inorganic matrix. (Figures 6 and A3). Using the highly concentrated suspensions (500 and 750 mg/L) resulted in the formation of a relatively dense coating of the silicon surface.

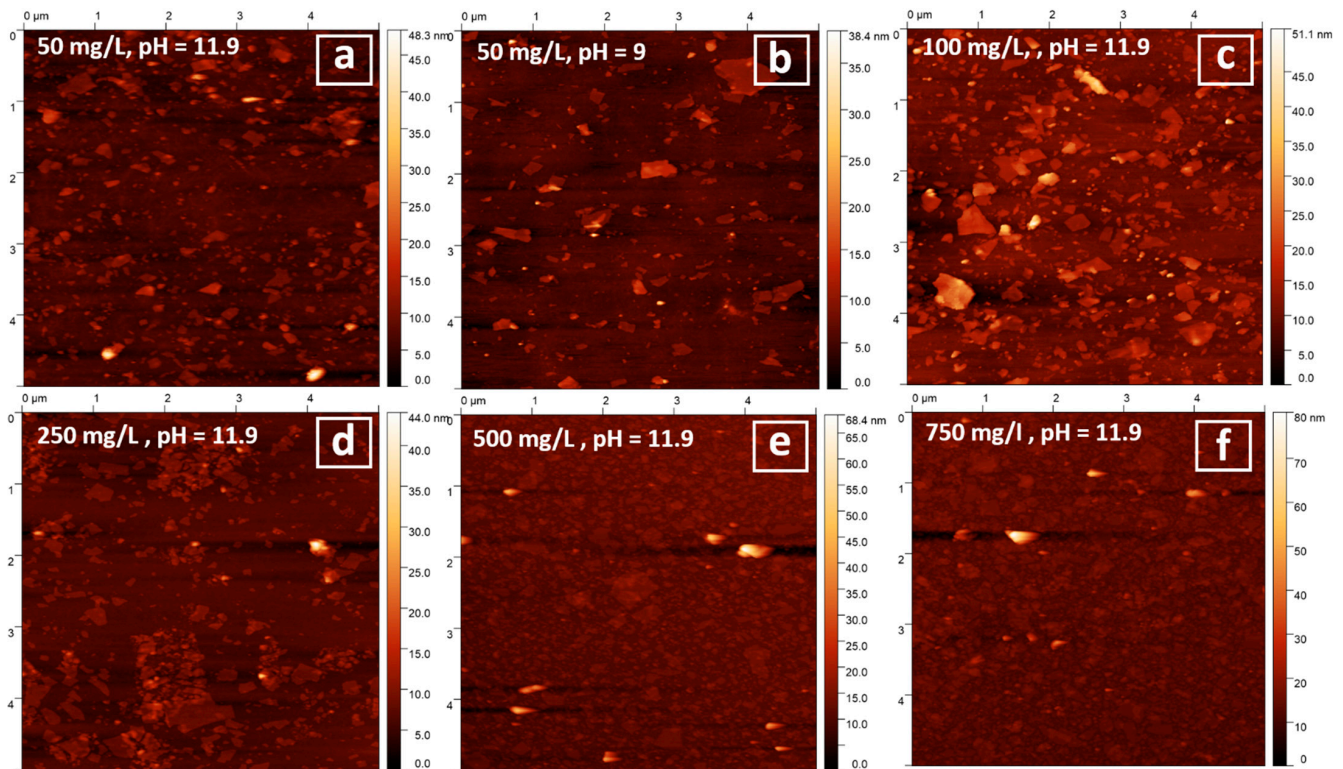


Figure 5. AFM images for coatings obtained in various conditions: 50 mg/L, pH 11.9 (a); 50 mg/L, pH 9 (b); 100 mg/L, pH 11.9 (c); 250 mg/L, pH 11.9 (d); 500 mg/L, pH 11.9 (e); 750 mg/L, pH 11.9 (f).

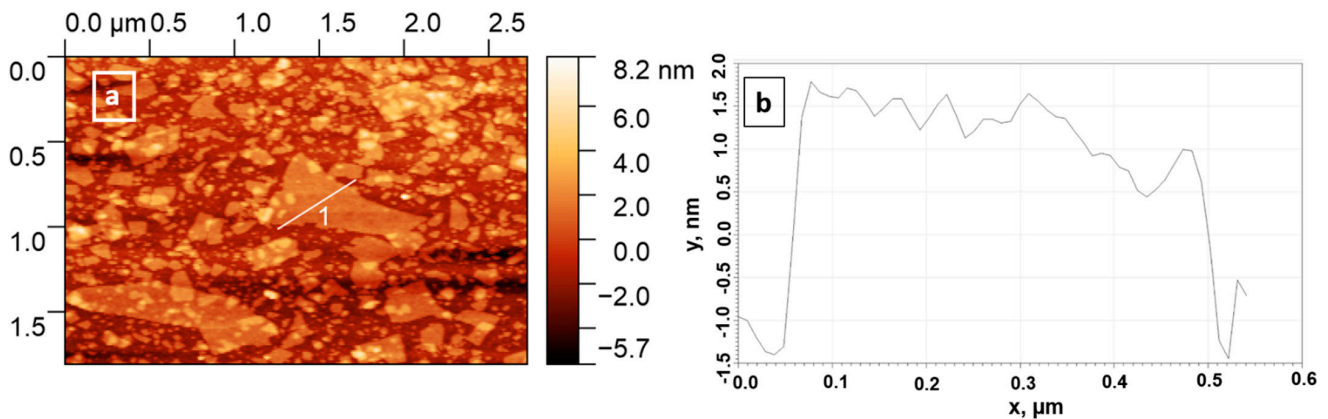


Figure 6. AFM image area (a) and height profile for a selected particle (b) for 500 mg/L, pH 11.9 suspension.

4. Conclusions

The physical–chemical exfoliation of a new Ruddlesden–Popper bismuth titanate, $\text{H}_2\text{K}_{0.5}\text{Bi}_{2.5}\text{Ti}_4\text{O}_{13}$, and its inorganic–organic hybrids with *n*-alkylamines was studied for the first time in an aqueous solution of TBAOH. Although it was possible to carry out the process of splitting and obtain a suspension of nanolayers for all samples, it was shown that the choice of precursor has a strong impact on the efficiency of exfoliation. To determine the concentration of the obtained suspensions, the two direct approaches—ICP analysis and the gravimetry method—were used. For express analysis, indirect UV–vis spectroscopy and the densimetry method were proposed. The most concentrated suspensions (up to 770 mg/L) after the removal of the unexfoliated part of oxide via centrifugation were obtained using the *n*-propylamine derivative. At the same time, the initially protonated derivative without intercalated amine was shown to have the worst exfoliation ability and stability of the

resulting suspension. No correlation was found between ζ -potentials of the suspensions obtained and their concentrations for various samples, which implies that the stability of the resultant suspension does not influence the exfoliation procedure, considering the possible precipitation of unstable exfoliated particles during the centrifugation. According to the DLS data for the suspension obtained from the *n*-propylamine derivative, the average particle size lies at around 65 nm, which is in agreement with SEM and AFM data for the deposited particles. The negatively charged nanosheets' deposition on the surface of the Si substrate coated with positively charged polymer, PEI, was studied, considering the concentration, and in some cases, the pH of the suspension. As a result, the dense coatings were obtained using suspensions with high concentrations for the first time for Ruddlesden–Popper-type titanates. The thickness of the major particles deposited was found to be around 2.5–3 nm, which corresponds to the single-layer thickness of the starting inorganic matrix; this indicates that under the conditions used, it is possible to obtain suspensions of monolayers of the corresponding oxide.

Thus, the results presented in this work expand the range of objects for the creation of oxide nanolayers. The resulting nanolayers and coatings can be used as functional materials for catalysis and electronics.

Author Contributions: Conceptualization, I.A.Z. and O.I.S.; methodology, I.A.M. and O.I.S.; investigation, I.A.M., S.A.K., V.V.G., V.D.K. and P.D.K.; writing—original draft preparation, I.A.M.; writing—review and editing, I.A.Z., S.A.K. and O.I.S.; supervision, I.A.Z.; project administration, I.A.Z.; funding acquisition, I.A.Z. and O.I.S. All authors have read and agreed to the published version of the manuscript.

Funding: This research was funded by the Russian Science Foundation, grant No. 20-73-00027 (the QCM-D experiments, surface coatings formation, and characterization methodology development) and by the Russian Foundation for Basic Research, grant No. 19-33-90050 (initial compound preparation, exfoliation, and sample characterization experiments).

Data Availability Statement: The data presented in this study are available in the article.

Acknowledgments: The study was conducted using the equipment of the Saint Petersburg State University Research Park: Centre for X-ray Diffraction Studies, Centre for Optical and Laser Research, Centre for Chemical Analysis and Materials Research, Centre for Thermal Analysis and Calorimetry, Interdisciplinary Centre for Nanotechnology, Centre for Innovative Technologies of Composite Nanomaterials, Centre for Diagnostics of Functional Materials for Medicine, Pharmacology and Nanoelectronics.

Conflicts of Interest: The authors declare no conflict of interest.

Appendix A

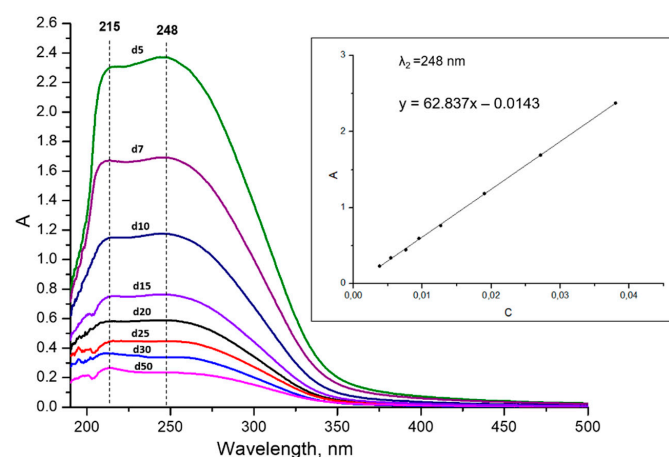


Figure A1. UV-vis spectra of $\text{HKBT}_4 \times \text{BuNH}_2$ suspensions in TBAOH with varied dilution and calibration obtained (inset). The initial concentration of undiluted suspension was 0.195 g/L.

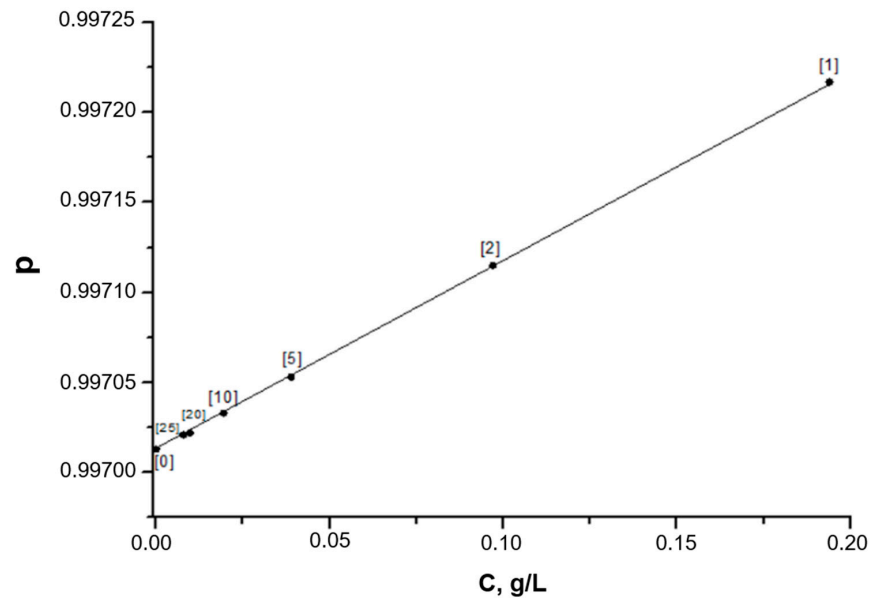


Figure A2. Density calibration obtained for $\text{HKBT}_4 \times \text{BuNH}_2$ suspension diluted to various concentrations (dilution degree presented in [] commas).

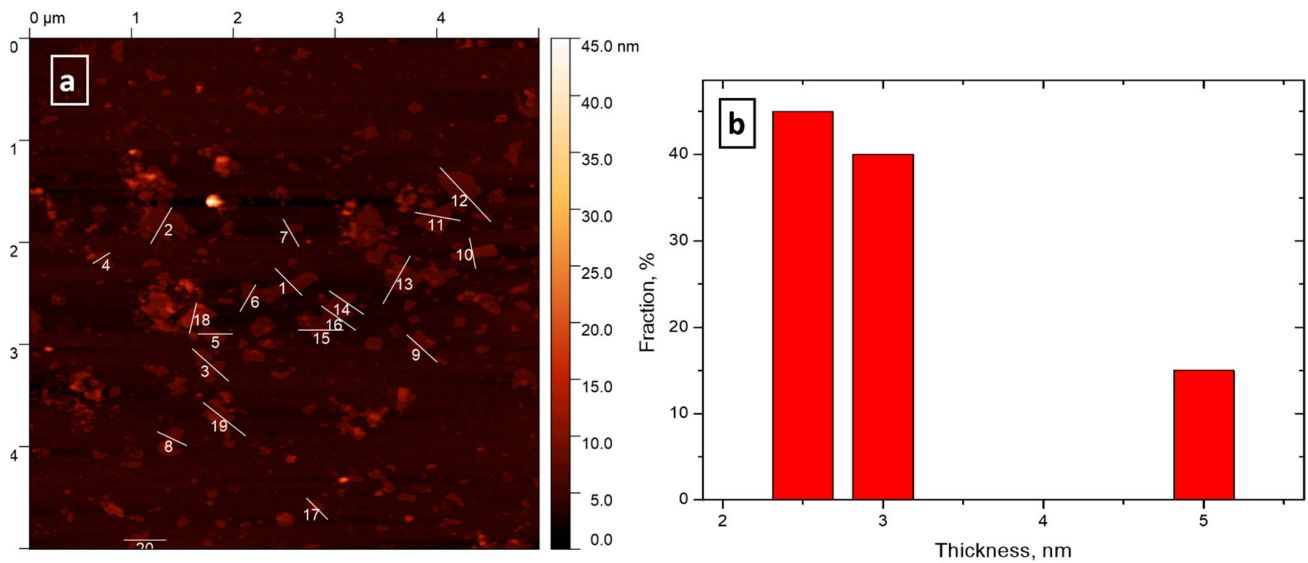


Figure A3. (a) AFM image for particles deposited from 250 mg/L suspension with marked particles used for thickness distribution calculations and (b) obtained thickness distribution.

References

- Geim, A.K.; Novoselov, K.S. The rise of graphene. *Nat. Mater.* **2007**, *6*, 183–191. [[CrossRef](#)] [[PubMed](#)]
- Dion, M.; Ganne, M.; Tournoux, M. Nouvelles familles de phases MIMII2Nb3O10 a feuillets “perovskites”. *Mater. Res. Bull.* **1981**, *16*, 1429–1435. [[CrossRef](#)]
- Jacobson, A.J.; Johnson, J.W.; Lewandowski, J.T. Interlayer Chemistry between Thick Transition-Metal Oxide Layers: Synthesis and Intercalation Reactions of $\text{K}[\text{Ca}_2\text{Na}_{n-3}\text{Nb}_n\text{O}_{3n+1}]$ ($3 \leq n \leq 7$). *Inorg. Chem.* **1985**, *24*, 3727–3729. [[CrossRef](#)]
- Kato, M.; Kajita, T.; Hanakago, R.; Koike, Y. Search for new superconductors by the Li-intercalation into layered perovskites. *Phys. C Supercond.* **2006**, *445–448*, 26–30. [[CrossRef](#)]
- Toda, K.; Teranishi, T.; Sato, M. Possibility of superconductivity in new reduced tantalate and titanate with the layered perovskite structure. *J. Eur. Ceram. Soc.* **1999**, *19*, 1525–1529. [[CrossRef](#)]
- Chen, C.; Ning, H.; Lepadatu, S.; Cain, M.; Yan, H.; Reece, M.J. Ferroelectricity in Dion–Jacobson ABiNb_2O_7 (A = Rb, Cs) compounds. *J. Mater. Chem. C* **2015**, *3*, 19–22. [[CrossRef](#)]
- Benedek, N.A. Origin of ferroelectricity in a family of polar oxides: The dion-jacobson phases. *Inorg. Chem.* **2014**, *53*, 3769–3777. [[CrossRef](#)]

8. Fennie, C.J.; Rabe, K.M. Ferroelectricity in the Dion-Jacobson CsBiNb₂O₇ from first principles. *Appl. Phys. Lett.* **2006**, *88*, 262902. [[CrossRef](#)]
9. Li, B.-W.; Osada, M.; Ebina, Y.; Ozawa, T.C.; Ma, R.; Sasaki, T. Impact of perovskite layer stacking on dielectric responses in KCa₂Na_{n-3}Nb_nO_{3n+1} (n = 3–6) Dion–Jacobson homologous series. *Appl. Phys. Lett.* **2010**, *96*, 182903. [[CrossRef](#)]
10. Gou, G.; Shi, J. Piezoelectricity enhancement in Dion-Jacobson RbBiNb₂O₇ via negative pressure. *EPL (Europhys. Lett.)* **2014**, *108*, 67006. [[CrossRef](#)]
11. Zhang, N.; Guo, C.; Jing, H. Photoluminescence and cathode-luminescence of Eu³⁺-doped NaLnTiO₄ (Ln = Gd and Y) phosphors. *RSC Adv.* **2013**, *3*, 7495. [[CrossRef](#)]
12. Gu, H.; Hu, Z.; Hu, Y.; Yuan, Y.; You, J.; Zou, W. The structure and photoluminescence of Bi₄Ti₃O₁₂ nanoplates synthesized by hydrothermal method. *Colloids Surf. A Physicochem. Eng. Asp.* **2008**, *315*, 294–298. [[CrossRef](#)]
13. Ida, S.; Ogata, C.; Eguchi, M.; Youngblood, W.J.; Mallouk, T.E.; Matsumoto, Y. Photoluminescence of perovskite nanosheets prepared by exfoliation of layered oxides, K₂Ln₂Ti₃O₁₀, KLnNb₂O₇, and RbLnTa₂O₇ (Ln: Lanthanide ion). *J. Am. Chem. Soc.* **2008**, *130*, 7052–7059. [[CrossRef](#)]
14. Rodionov, I.A.; Silyukov, O.I.; Zvereva, I.A. Study of photocatalytic activity of layered oxides: NaNdTiO₄, LiNdTiO₄, and HNdTiO₄ titanates. *Russ. J. Gen. Chem.* **2012**, *82*, 635–638. [[CrossRef](#)]
15. Domen, K.; Yoshimura, J.; Sekine, T.; Kondo, J.; Tanaka, A.; Maruya, K.; Onishi, T. A Novel Series of Photocatalysts with an Ion-Exchangeable Layered Structure of Niobate. *Stud. Surf. Sci. Catal.* **1993**, 2159–2162. [[CrossRef](#)]
16. Hu, Y.; Mao, L.; Guan, X.; Tucker, K.A.; Xie, H.; Wu, X.; Shi, J. Layered perovskite oxides and their derivative nanosheets adopting different modification strategies towards better photocatalytic performance of water splitting. *Renew. Sustain. Energy Rev.* **2020**, *119*, 109527. [[CrossRef](#)]
17. Rodionov, I.A.; Silyukov, O.I.; Utkina, T.D.; Chislov, M.V.; Sokolova, Y.P.; Zvereva, I.A. Photocatalytic properties and hydration of perovskite-type layered titanates A₂Ln₂Ti₃O₁₀ (A = Li, Na, K; Ln = La, Nd). *Russ. J. Gen. Chem.* **2012**, *82*, 1191–1196. [[CrossRef](#)]
18. Lichtenberg, F.; Herrnberger, A.; Wiedenmann, K. Synthesis, structural, magnetic and transport properties of layered perovskite-related titanates, niobates and tantalates of the type A_nB_nO_{3n+2}, A'_{A_{k-1}}B_kO_{3k+1} and A_mB_{m-1}O_{3m}. *Prog. Solid State Chem.* **2008**, *36*, 253–387. [[CrossRef](#)]
19. Yang, Y.; Chen, Q.; Yin, Z.; Li, J. Study on the photocatalytic activity of K₂La₂Ti₃O₁₀ doped with vanadium (V). *J. Alloys Compd.* **2009**, *488*, 364–369. [[CrossRef](#)]
20. Ozawa, T.C.; Fukuda, K.; Akatsuka, K.; Ebina, Y.; Sasaki, T. Preparation and Characterization of the Eu³⁺ Doped Perovskite Nanosheet Phosphor: La_{0.90}Eu_{0.05}Nb₂O₇. *Chem. Mater.* **2007**, *19*, 6575–6580. [[CrossRef](#)]
21. Wei, T.; Li, C.P.; Zhou, Q.J.; Zou, Y.L.; Zhang, L.S. Upconversion luminescence and ferroelectric properties of Er³⁺ doped Bi₄Ti₃O₁₂–SrBi₄Ti₄O₁₅. *Mater. Lett.* **2014**, *118*, 92–95. [[CrossRef](#)]
22. Ya-Hui, Y.; Qi-Yuan, C.; Zhou-Lan, Y.; Jie, L. Study on the photocatalytic activity of K₂La₂Ti₃O₁₀ doped with zinc(Zn). *Appl. Surf. Sci.* **2009**, *255*, 8419–8424. [[CrossRef](#)]
23. Huang, Y.; Xie, Y.; Fan, L.; Li, Y.; Wei, Y.; Lin, J.; Wu, J. Synthesis and photochemical properties of La-doped HCa₂Nb₃O₁₀. *Int. J. Hydrog. Energy* **2008**, *33*, 6432–6438. [[CrossRef](#)]
24. Gopalakrishnan, J. Chimie Douce Approaches to the Synthesis of Metastable Oxide Materials. *Am. Chem. Soc.* **1995**, *7*, 1265–1275. [[CrossRef](#)]
25. Schaak, R.E.; Mallouk, T.E. Perovskites by Design: A Toolbox of Solid-State Reactions. *Chem. Mater.* **2002**, *14*, 1455–1471. [[CrossRef](#)]
26. Yafarova, L.V.; Silyukov, O.I.; Myshkovskaya, T.D.; Minich, I.A.; Zvereva, I.A. New data on protonation and hydration of perovskite-type layered oxide KCa₂Nb₃O₁₀. *J. Therm. Anal. Calorim.* **2021**, *143*, 87–93. [[CrossRef](#)]
27. Jacobson, A.J.; Johnson, J.W.; Lewandowski, J. Intercalation of the layered solid acid HCa₂Nb₃O₁₀ by organic amines. *Mater. Res. Bull.* **1987**, *22*, 45–51. [[CrossRef](#)]
28. Hong, Y.; Kim, S.-J. Intercalation of Primary Diamines in the Layered Perovskite Oxides, HSr₂Nb₃O₁₀. *Bull. Korean Chem. Soc.* **1996**, *17*, 730–735.
29. Kurnosenko, S.A.; Silyukov, O.I.; Mazur, A.S.; Zvereva, I.A. Synthesis and thermal stability of new inorganic-organic perovskite-like hybrids based on layered titanates HLnTiO₄ (Ln = La, Nd). *Ceram. Int.* **2020**, *46*, 5058–5068. [[CrossRef](#)]
30. Silyukov, O.I.; Khramova, A.D.; Zvereva, I.A. Synthesis of Organic-Inorganic Derivatives of Perovskite-Like Layered HCa₂Nb₃O₁₀ Oxide with Monoethanolamine and Glycine. *Glas. Phys. Chem.* **2020**, *46*, 256–259. [[CrossRef](#)]
31. Wang, T.H.; Henderson, C.N.; Draskovic, T.I.; Mallouk, T.E. Synthesis, exfoliation, and electronic/protonic conductivity of the dion-jacobson phase layer perovskite HLa₂TiTa₂O₁₀. *Chem. Mater.* **2014**, *26*, 898–906. [[CrossRef](#)]
32. Nicolosi, V.; Chhowalla, M.; Kanatzidis, M.G.; Strano, M.S.; Coleman, J.N. Liquid Exfoliation of Layered Materials. *Science* **2013**, *340*, 1226419. [[CrossRef](#)]
33. Osada, M.; Sasaki, T. Exfoliated oxide nanosheets: New solution to nanoelectronics. *J. Mater. Chem.* **2009**, *19*, 2503–2511. [[CrossRef](#)]
34. Lee, W.-J.; Yeo, H.J.; Kim, D.-Y.; Paek, S.-M.; Kim, Y.-I. Exfoliation of Dion-Jacobson Layered Perovskite into Macromolecular Nanoplatelet. *Bull. Korean Chem. Soc.* **2013**, *34*, 2041–2043. [[CrossRef](#)]
35. Li, B.-W.; Osada, M.; Akatsuka, K.; Ebina, Y.; Ozawa, T.C.; Sasaki, T. Solution-Based Fabrication of Perovskite Multilayers and Superlattices Using Nanosheet Process. *Jpn. J. Appl. Phys.* **2011**, *50*, 09NA10. [[CrossRef](#)]

36. Pulyalina, A.; Rostovtseva, V.; Minich, I.; Silyukov, O.; Toikka, M.; Saprykina, N.; Polotskaya, G. Specific Structure and Properties of Composite Membranes Based on the Torlon® (Polyamide-imide)/Layered Perovskite Oxide. *Symmetry* **2020**, *12*, 1142. [[CrossRef](#)]
37. Sasaki, T.; Ebina, Y.; Tanaka, T.; Harada, M.; Watanabe, M.; Decher, G. Layer-by-layer assembly of titania nanosheet/polycation composite films. *Chem. Mater.* **2001**, *13*, 4661–4667. [[CrossRef](#)]
38. Hong, Y.-S.; Kim, S.-J. Synthesis and Characterization of Molecular Composite Prepared from Layered Perovskite Oxide, $\text{HLa}_2\text{Ti}_2\text{NbO}_{10}$. *Bull. Korean Chem. Soc.* **1997**, *18*, 623–628. [[CrossRef](#)]
39. Ida, S.; Ogata, C.; Unal, U.; Izawa, K.; Inoue, T.; Altuntasoglu, O.; Matsumoto, Y. Preparation of a blue luminescent nanosheet derived from layered perovskite $\text{Bi}_2\text{SrTa}_2\text{O}_9$. *J. Am. Chem. Soc.* **2007**, *129*, 8956–8957. [[CrossRef](#)]
40. Tetsuka, H.; Takashima, H.; Ikegami, K.; Nanjo, H.; Ebina, T.; Mizukami, F. Nanosheet seed-layer assists oriented growth of highly luminescent perovskite films. *Chem. Mater.* **2009**, *21*, 21–26. [[CrossRef](#)]
41. Takagaki, A.; Sugisawa, M.; Lu, D.; Kondo, J.N.; Hara, M.; Domen, K.; Hayashi, S. Exfoliated nanosheets as a new strong solid acid catalyst. *J. Am. Chem. Soc.* **2003**, *125*, 5479–5485. [[CrossRef](#)]
42. Zhou, Y.; Wen, T.; Zhang, X.; Chang, B.; Kong, W.; Guo, Y.; Yang, B.; Wang, Y. A Multiple Structure-Design Strategy towards Ultrathin Niobate Perovskite Nanosheets with Thickness-Dependent Photocatalytic Hydrogen-Evolution Performance. *Chem.-Asian J.* **2017**, *12*, 2727–2733. [[CrossRef](#)]
43. Hu, S.; Chi, B.; Pu, J.; Jian, L. Novel heterojunction photocatalysts based on lanthanum titanate nanosheets and indium oxide nanoparticles with enhanced photocatalytic hydrogen production activity. *J. Mater. Chem. A* **2014**, *2*, 19260–19267. [[CrossRef](#)]
44. Osada, M.; Akatsuka, K.; Ebina, Y.; Kotani, Y.; Ono, K.; Funakubo, H.; Ueda, S.; Kobayashi, K.; Takada, K.; Sasaki, T. Langmuir–Blodgett Fabrication of Nanosheet-Based Dielectric Films without an Interfacial Dead Layer. *Jpn. J. Appl. Phys.* **2008**, *47*, 7556–7560. [[CrossRef](#)]
45. Khan, M.S.; Kim, H.; Kim, Y.; Ebina, Y.; Sugimoto, W.; Sasaki, T.; Osada, M. Scalable Design of Two-Dimensional Oxide Nanosheets for Construction of Ultrathin Multilayer Nanocapacitor. *Small* **2020**, *16*, 2003485. [[CrossRef](#)] [[PubMed](#)]
46. Liu, S.; Avdeev, M.; Liu, Y.; Johnson, M.R.; Ling, C.D. A New $n = 4$ Layered Ruddlesden–Popper Phase $\text{K}_{2.5}\text{Bi}_{2.5}\text{Ti}_4\text{O}_{13}$ Showing Stoichiometric Hydration. *Inorg. Chem.* **2016**, *55*, 1403–1411. [[CrossRef](#)] [[PubMed](#)]
47. Silyukov, O.I.; Minich, I.A.; Zvereva, I.A. Synthesis of protonated derivatives of layered perovskite-like bismuth titanates. *Glas. Phys. Chem.* **2018**, *44*, 115–119. [[CrossRef](#)]
48. Minich, I.A.; Silyukov, O.I.; Kulish, L.D.; Zvereva, I.A. Study on thermolysis process of a new hydrated and protonated perovskite-like oxides $\text{H}_2\text{K}_{0.5}\text{Bi}_{2.5}\text{Ti}_4\text{O}_{13} \cdot y\text{H}_2\text{O}$. *Ceram. Int.* **2019**, *45*, 2704–2709. [[CrossRef](#)]
49. Minich, I.A.; Silyukov, O.I.; Gak, V.V.; Borisov, E.V.; Zvereva, I.A. Synthesis of Organic-Inorganic Hybrids Based on Perovskite-like Bismuth Titanate $\text{H}_2\text{K}_{0.5}\text{Bi}_{2.5}\text{Ti}_4\text{O}_{13} \cdot \text{H}_2\text{O}$ and n -Alkylamines. *ACS Omega* **2020**, *5*, 8158–8168. [[CrossRef](#)]
50. Minich, I.A.; Silyukov, O.I.; Mazur, A.S.; Zvereva, I.A. Grafting reactions of perovskite-like bismuth titanate $\text{H}_2\text{K}_{0.5}\text{Bi}_{2.5}\text{Ti}_4\text{O}_{13} \cdot \text{H}_2\text{O}$ with n -alcohols. *Ceram. Int.* **2020**, *46*, 29373–29381. [[CrossRef](#)]
51. Ebina, Y.; Sasaki, T.; Watanabe, M. Study on exfoliation of layered perovskite-type niobates. *Solid State Ion.* **2002**, *151*, 177–182. [[CrossRef](#)]
52. Gao, H.; Shori, S.; Chen, X.; zur Loye, H.C.; Ploehn, H.J. Quantitative analysis of exfoliation and aspect ratio of calcium niobate platelets. *J. Colloid Interface Sci.* **2013**, *392*, 226–236. [[CrossRef](#)] [[PubMed](#)]
53. Ebina, Y.; Akatsuka, K.; Fukuda, K.; Sasaki, T. Synthesis and in situ X-ray diffraction characterization of two-dimensional perovskite-type oxide colloids with a controlled molecular thickness. *Chem. Mater.* **2012**, *24*, 4201–4208. [[CrossRef](#)]
54. Kurnosenko, S.A.; Silyukov, O.I.; Minich, I.A.Z. Exfoliation of Methylamine and n -Butylamine Derivatives of Layered Perovskite-Like Oxides HLnTiO_4 and $\text{H}_2\text{Ln}_2\text{Ti}_3\text{O}_{10}$ ($\text{Ln} = \text{La}, \text{Nd}$) into Nanolayers. *Glas. Phys. Chem.* **2021**, *47*, 372–381. [[CrossRef](#)]
55. Li, S.; Leroy, P.; Heberling, F.; Devau, N.; Jougnot, D.; Chiaberge, C. Influence of surface conductivity on the apparent zeta potential of calcite. *J. Colloid Interface Sci.* **2016**, *468*, 262–275. [[CrossRef](#)]
56. Tantra, R.; Schulze, P.; Quincey, P. Effect of nanoparticle concentration on zeta-potential measurement results and reproducibility. *Particuology* **2010**, *8*, 279–285. [[CrossRef](#)]
57. Suh, J.; Hwang, B.K. Ionization of PEI and PAA at various pH's. *Bioorg. Chem.* **1994**, *22*, 318–327. [[CrossRef](#)]